Regular Article – Atomic and Molecular Collisions

Electron-impact excitation of the $5\,^2\mathrm{S}_{1/2} \to 5\,^2\mathrm{P}_{1/2}$ and $5\,^2\mathrm{P}_{3/2}$ transitions in rubidium by 40 eV electrons: theory and experiment

K. R. Hamilton[1], O. Zatsarinny[1], K. Bartschat[1], B. Predojević[2,3], D. Šević[2], B. P. Marinković[2], and M. J. Brunger[4,5,a]

[1] Department of Physics and Astronomy, Drake University, Des Moines, IA 50311, USA
[2] Institute of Physics Belgrade, University of Belgrade, Pregrevica 118, Belgrade 11080, Serbia
[3] Faculty of Natural Sciences, University of Banja Luka, 78000 Banja Luka, Republic of Srpska, Bosnia and Herzegovina
[4] College of Science and Engineering, Flinders University, GPO Box 2100, Adelaide, SA 5001, Australia
[5] Institute of Actuarial Science and Data Analytics, UCSI University, 56000 Kuala Lumpur, Malaysia

Abstract. We report on a series of detailed Breit-Pauli and Dirac B-spline R-matrix (DBSR) differential cross section (DCS) calculations for excitation of the $5\,^2\mathrm{S}_{1/2} \to 5\,^2\mathrm{P}_{1/2}$ and $5\,^2\mathrm{S}_{1/2} \to 5\,^2\mathrm{P}_{3/2}$ states in rubidium by 40 eV incident electrons. The early BP computations shown here were carried out with both 5 states and 12 states, while the DBSR models coupled 150 and 325 states, respectively. We also report corresponding results from a limited set of DCS measurements on the unresolved $5\,^2\mathrm{P}_{1/2,3/2}$ states, with the experimental data being restricted to the scattered electron angular range 2–10°. Typically, good agreement is found between our calculated and measured DCS for excitation of the unresolved $5\,^2\mathrm{P}_{1/2,3/2}$ states, with best accord being found between the DBSR predictions and the measured data. The present theoretical and experimental results are also compared with predictions from earlier 40 eV calculations using the nonrelativistic Distorted-Wave Born Approximation and a Relativistic Distorted-Wave model.

1 Introduction

The electronic structure of the ground state of the alkali metals, of which rubidium (Rb) is a member, consists of one valence electron outside a core, which is a system of configuration $n\mathrm{p}^6(n+1)\mathrm{s}$. Alkali metals belong to Group I of the Periodic Table, as does atomic hydrogen (H). However, the outer electron of the alkali metals moves in a spherically symmetric potential, which differs from the pure Coulomb interaction in H. As a consequence, for small values of the orbital angular momentum quantum number (ℓ) in the alkali metals, there is a closer approach of the outer electrons to the nucleus. This causes the screening to decrease while the proximity of the outer electrons distorts the core in a way that might be seen as an electrostatic polarization. This electronic structure makes alkali metals very interesting for both theoretical and experimental investigation.

Despite the intrinsic theoretical and experimental interest in Rb, relatively little work has thus far been reported in respect to inelastic electron interactions

with Rb vapour. Vušković et al. [1] reported measurements of both DCS and integral cross sections, for electron impact excitation of the unresolved $5\,^2\mathrm{S}_{1/2} \to 5\,^2P_{1/2,3/2}$ transition, at energies of 10 eV, 20 eV, and 200 eV and for scattering angles ranging from 5° to 120°. Their measured relative DCSs were placed on an absolute scale through a normalization procedure using the optical oscillator strength for that transition [2]. However, as discussed in references [3,4], some of their pioneering work should be treated with caution, and we suspect that this is also likely the case here. Corresponding Distorted-Wave Born Approximation (DWBA) results were calculated originally by Pangatiwar and Srivastava [5], later updated by Saxena and Srivastava [6], and results from an even later Relativistic Distorted-Wave (RDW) approximation calculation from Zeman et al. [7] are also noted. Superelastic electron scattering from the resonance line has also been investigated by Hall et al. [8], while asymmetries in the scattering of spin-polarized electrons from Rb were studied by Guinea et al. [9]. A theoretical analysis of channel coupling and relativistic effects in the excitation of the Rb resonance line by Payne et al. [10], using a Breit-Pauli (BP) R-matrix (close-coupling) method, has also been reported. Further, we note the coupled-

O. Zatsarinny: deceased.

[a] e-mail: Michael.Brunger@flinders.edu.au (corresponding author)

channel optical potential method (CCOM) theory, at 20 eV, from Chin et al. [11]. Finally, for completeness, we note a study into the ionization of Rb by 50-eV electron impact, from Haynes et al. [12].

There has also been very recent interest [13] in investigating interference between some Rb line coherences, in order to study so-called exceptional points, which are essentially singularities in the response of coupled oscillators. Coupled oscillators are prevalent in nature and fundamental in a wide range of fields, including photonics [14], geophysics, and astrophysics. In particular, with respect to photonics, two-photon Rb spectroscopy, in conjunction with an exposed-core optic-fibre platform, was studied as a source to produce on-demand and deterministic entanglement [14].

The remainder of this manuscript is structured as follows. In Sect. 2 we provide a brief description of our experimental methods and analysis, while in Sect. 3 some details of our BP and Dirac B-spline R-matrix (DBSR) calculations are given. Thereafter, in Sect. 4, our results and a discussion of those results are presented, followed by some conclusions from this investigation being drawn in Sect. 5.

2 Experimental considerations

The apparatus employed in the present measurements is a conventional crossed-beam spectrometer, the details of which can be found elsewhere [3,4,15]. Briefly, a nearly monoenergetic beam of electrons intersected a beam of Rb atoms at right angles. The incident electrons were generated by an electron monochromator, consisting of cylindrical electrostatic lens elements and a hemispherical energy selector. The scattered electrons were detected by a channeltron placed at the exit of an electrostatic analyser system, which also incorporates a hemispherical energy selector and some cylindrical electrostatic lens elements. The effusive atomic beam was generated by resistively heating an oven containing high-purity Rb. The vertical oven crucible was heated by two separate elements, which provided a temperature difference between the top and bottom of the oven, with the aim being to prevent clogging of the cylindrical-symmetry beam-former.

The measurements were performed at a temperature of 510 K, which corresponds to a metal-vapour pressure of approximately 18 Pa. At this temperature, the number density of Rb effusing through the cylindrical beam-former (aspect ratio $\gamma = 0.075$) was 10^{15}–10^{16} cm^{-3} going from the crucible into the interaction volume. The true zero electron scattering angle (θ) was determined on the basis of the symmetry of the inelastically scattered electron intensity (for the excitation of the unresolved $5\,^2P_{1/2,3/2}$ states), to within a 0.2° uncertainty. The angular resolution of the analyser was estimated to be 1.5° (FWHM), while the overall system energy resolution was typically ∼160 meV (FWHM) in these measurements. The energy scale was calibrated
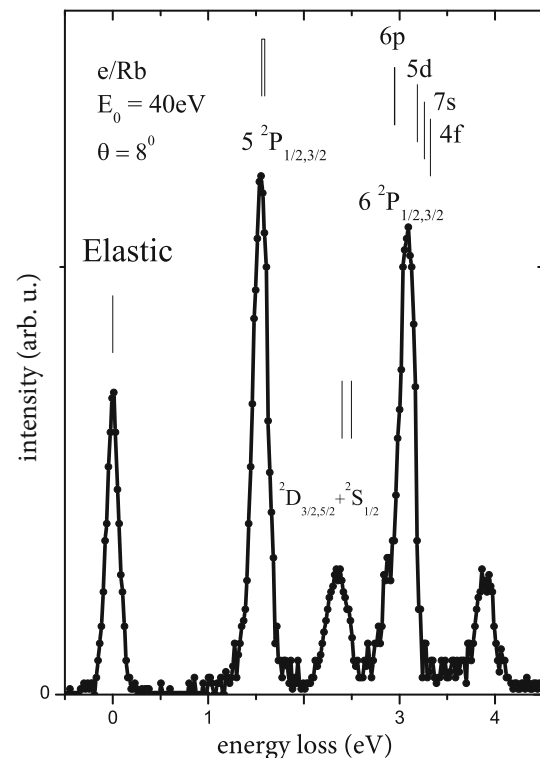
Fig. 1 Typical energy loss spectrum for electron scattering from rubidium. The incident electron energy was $E_0 = 40$ eV and the scattered electron angle was $\theta = 8°$. The spectroscopic notation for the main features is indicated. The solid black line is a weighted cubic-spline interpolation between the data points

as in reference [15], with an uncertainty in that process of ± 0.1 eV.

Before each angular distribution measurement (i.e., the scattered intensity as a function of θ), we recorded an electron energy-loss spectrum (see Fig. 1), to both verify that the $5\,^2P_{1/2,3/2}$ peak was well separated from the elastic channel and the other excited inelastic states, and to verify the absence of double scattering. The position of the analyser was varied from approximately $\theta° = -12°$ to $+12°$, and the $5\,^2P_{1/2,3/2}$ angular distribution was measured. We had intended to measure the angular distribution over a much larger scattered electron angular and energy range, but due to an unexpected and catastrophic system failure, which could not be rectified despite attempts to do so, the present experimental measurements were limited to near-forward θ and a single energy (E_0) of 40 eV. That angular distribution was subsequently corrected using effective path-length correction factors, following the approach of Brinkman and Trajmar [16], to determine the relative DCS.

The relative DCS was then placed on an absolute scale using the forward-angle scattering function (FSF) method, as introduced by Avdonina et al. [17], where the recent work of Safronova and colleagues [18] was employed to determine an optical oscillator strength (OOS) value of 1.0231 for the $5\,^2P_{1/2,3/2}$ excitation.

Table 1 Experimental differential cross sections $(10^{-16} \text{cm}^2/\text{sr})$ for 40 eV electron-impact excitation of the $5\,^2\text{S}_{1/2} \rightarrow 5\,^2P$ transition in Rb. The stated uncertainties are at the one standard deviation level

Scattering Angle (deg)	DCS $(10^{-16}\text{cm}^2/\text{sr})$	Error in DCS
2	1749	263
4	480	72
6	173	26
8	79.1	12.5
10	40.5	6.8

That value is expected to be more accurate than the earlier OOS result from Steck [19], of 1.0376 ± 0.0029, which is in turn more reliable than the OOS result from Dalgarno and Davison [20] who suggested a value of 1.06 ± 0.01. Note that at least some of the error on the absolute cross sections in Vušković et al. [1] might be ascribed to the inaccuracy of the OOS values that were available at that time.

Contributions to the total error on the absolute DCS come from: (a) uncertainties in our experimental values and (b) uncertainty in our normalization procedure. The uncertainties in our experimental values arise from statistical uncertainties, errors in the application of the effective path-length correction factor (6%), an uncertainty in our energy calibration (1%), and in the calibration of the true 0° scattering angle (3%). The uncertainty in the normalization (10%) arises from an uncertainty in the OOS (less than 1%) and in the fitting of the FSF. The total errors on the absolute DCS are formed from the square root of the sum of the squared individual uncertainties. The present measured absolute DCS and their associated uncertainties are given in Table 1.

3 Theoretical details

For this paper, we extended the earlier semi-relativistic Breit-Pauli R-matrix (close-coupling) calculations reported by Payne et al. [10] to a full-relativistic framework with a larger number of pseudo-states. Specifically, we used the Dirac B-Spline R-matrix (DBSR) approach described by Zatsarinny and Bartschat [21] and then employed for e-Cs collisions. Even though Rb with a nuclear charge of $Z = 37$ is one row above Cs $(Z = 55)$ in the periodic table, and hence relativistic effects are likely less important for scattering from this target, we will see that they can become significant under certain conditions, especially when the cross sections are small and hence become highly sensitive to details in the theoretical model.

The present results were obtained with 150 and 325 states, respectively, included in the two close-coupling models labelled DBSR-150 and DBSR-325 below. In the latter model, the number of target states (physical plus pseudo) for the various partial-wave symmetries with total electronic angular momentum J and parity $\pi = \pm$ was:

$(1/2)^+{:}43;\ (1/2)^-{:}46;\ (3/2)^+{:}43;\ (3/2)^-{:}59;\ (5/2)^+{:}50;$ $(5/2)^-{:}35;\ (7/2)^+{:}23;\ (7/2)^-{:}17;\ (9/2)^+{:}9.$

Most of the states had the valence configuration $4\text{p}^6 n\ell$ with $\ell = 0-4$, but some states with $4\text{p}^5 n_1\ell_1 n_2\ell_2$ were also constructed in order to properly account for the polarizability of the core and to include important auto-ionizing states [22]. The R-matrix radius was set to 50 a_0, where $a_0 = 0.529 \times 10^{-10}$ m is the Bohr radius. The region was spanned by 109 splines of orders 8 and 9 each for the large and the small components of the orbitals, respectively. Using different spline orders avoids the occurrence of spurious states [23]. With this distribution, 32 states had energies below the ionization threshold, while the remaining ones represented the coupling to the ionization continuum. The highest pseudo-state had an energy of ≈ 22 eV. Experience shows that this should be sufficient to account for the relevant coupling and also provide reliable total ionization cross sections. The lowest 12–15 states are accurate representations of the true physical target states, while the remaining states with energies below the ionization threshold represent the coupling to the Rydberg continuum.

For the present case of interest, the DBSR-325 as well as the DBSR-150 model (where the number of states was roughly cut in half per J^π symmetry across the board) is almost certainly more than sufficient, as we will show by comparing the results with predictions from the much simpler 5-state (BPRM-5) and 12-state (BPRM-12) Breit-Pauli models. In BPRM-5, only the physical states $(5\text{s})^2 S_{1/2}$, $(5\text{p})^2 P_{1/2,3/2}$, and $(4\text{d})^2 D_{3/2,5/2}$ were coupled, while the close-coupling expansion was augmented with $(6\text{s})^2 S_{1/2}$, $(6\text{p})^2 P_{1/2,3/2}$, $(5\text{d})^2 D_{3/2,5/2}$, and $(4\text{f})^2 F_{5/2,7/2}$ in BPRM-12. Such models are expected to be more or less sufficient for elastic scattering as well as electron-impact excitation of the strong $(5\text{s})^2 S_{1/2} \rightarrow (5\text{p})^2 P_{1/2,3/2}$ resonance transitions, due to the small energy gap for excitation (less than 1.6 eV) and the fact that the dipole polarizability of the ground state originates almost entirely from the coupling to the $(5\text{p})^2 P_{1/2,3/2}$ states.

However, results from BPRM-5, BPRM-12, and even the earlier more extensive BP-models with a few more (pseudo-)states are not extensive enough to enable the modelling of a dipole-pumped alkali laser (DPAL) based on Rb rather than the one described for Cs by Zatsarinny et al. [24]. In order to provide datasets for an Rb-based DPAL, we set up the more extensive DBSR calculations, which can provide results for transitions between many discrete states as well as electron-induced bound-continuum transitions to give ionization cross sections from the ground state as well as selected excited states. These calculations are much more computationally expensive. Pushing them to an energy as high as 40 eV is not trivial. Here we calculated partial waves up to a total electronic angular momentum $J_{\max} = 25$ of the projectile+target collision

system, and then used an extrapolation procedure to ensure the convergence of the partial-wave expansions. To check the accuracy, we started the extrapolation at several smaller values of $J_{\max}$ to ensure that the results did not change significantly.

4 Results and discussion

Figure 2 shows our theoretical predictions for electron-impact excitation of the $(5s)^2S_{1/2} \rightarrow (5p)^2P_{1/2,3/2}$ transitions, as obtained in the BPRM-5, BPRM-12, DBSR-150, and DBSR-325 models, respectively. As expected, the DCS is dominated by small angles, dropping by more than two orders of magnitude between the 0 and 10°. When the full range of angles is plotted, the only differences larger than the thickness of the lines are the details of the shoulder between about 20 and 50°, as well as the minima around 60° and 145°. One of the key features in Fig. 2 is the oscillatory nature of the calculated angular distributions. This oscillatory behaviour appears to be ubiquitous in electron collision processes, for both the elastic and discrete inelastic
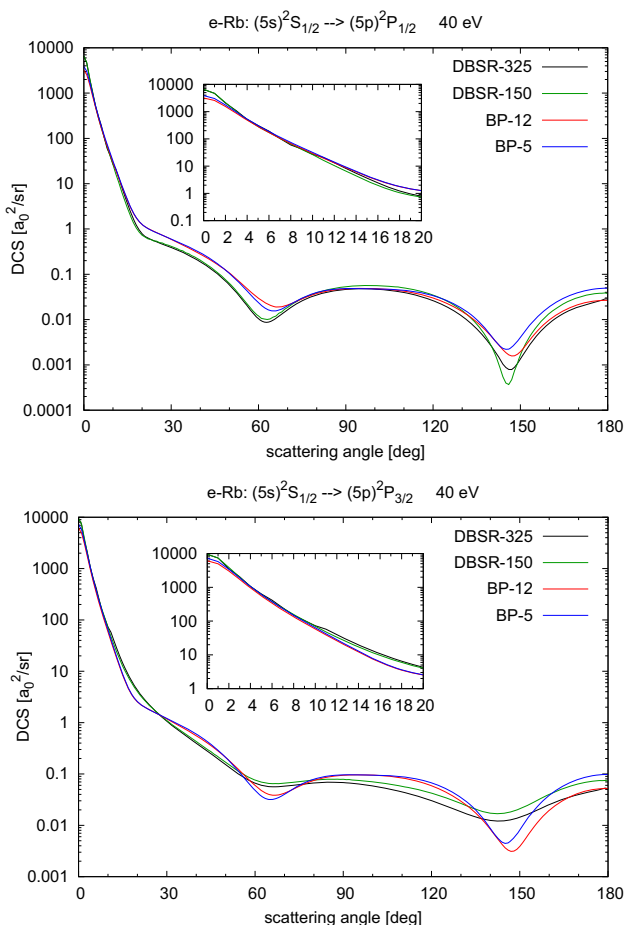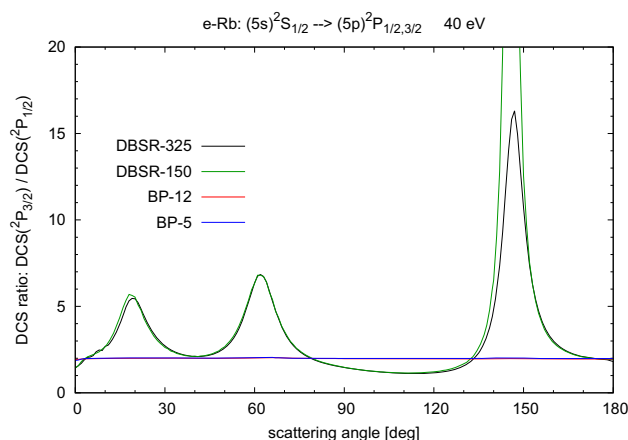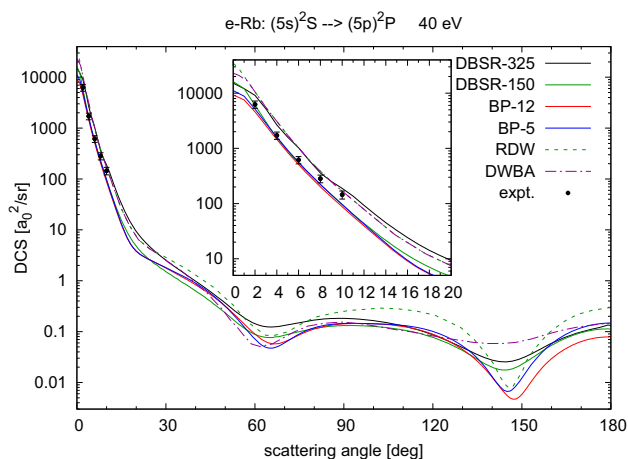

Fig. 3 Ratio of the DCSs for the $(5s)^2S_{1/2} \rightarrow (5p)^2P_{3/2}$ and $(5s)^2S_{1/2} \rightarrow (5p)^2P_{1/2}$ transitions in various DBSR and BPRM models described in the text. The purely statistical ratio is 2

channels. Some specific examples for electron scattering from metal vapours include zinc [3], bismuth [4], silver [15], sodium [25], magnesium [26] and indium [27]. The oscillatory nature of any differential cross section arises from the interference, both constructive and destructive, between the various partial waves that describe the collisional behaviour [28]. In the present case of inelastic scattering, where the orbital angular momentum of the projectile necessarily has to change from the initial state to the final state in order to conserve the parity as well as the coupled electronic angular momentum of the combined target + projectile collision system, the details depend in a complex way on the interference between T-matrix elements that need to be combined with spherical harmonics in order to generate the scattering amplitudes [29] and, subsequently, the differential cross section [30]. It is, hence, generally impossible to predict either the number or the positions of the minima (maxima) in the angular distributions. Even though in some special circumstances and models a resemblance to elastic scattering may appear in inelastic collisions [31,32], and the DCS generally exhibits less structure in the angular dependence with decreasing projectile energy, drawing truly quantitative conclusions is simply not feasible [33].

From a theoretical point of view, the most interesting result might be seen in Fig. 3, which exhibits the ratio of the differential cross sections for excitation of the two fine-structure states. Since the number of magnetic sublevels for each of those states is $2J_t + 1$, where J_t is the total electronic angular momentum of the fine-structure state, the statistical ratio to be expected is $r = 2$. This is exact if (i) the energy difference is zero and (ii) there are no explicitly spin-dependent interactions on the projectile electron. These ratios can be very sensitive to details of the theoretical model. For two examples, see the recent studies on the noble gases Kr [34] and Xe [35], where the fine-structure is easier to resolve in the electronic channel than in the alkalis

Fig. 2 DCS for the $(5s)^2S_{1/2} \rightarrow (5p)^2P_{1/2}$ (top) and $(5s)^2S_{1/2} \rightarrow (5p)^2P_{3/2}$ (bottom) transitions in various DBSR and BPRM models described in the text

Fig. 4 DCS for the $(5s)^2S_{1/2} \rightarrow (5p)^2P$ transition with unresolved fine-structure, as obtained in various DBSR and BPRM models described in the text. Also shown are predictions from two distorted-wave calculations

such as Rb. It is noteworthy that the two BPRM calculations, indeed, predict the ratio to be very close to 2, while the DBSR models indicate significant deviations from that statistical ratio, especially near the minima of the DCS but also around the start of the first shoulder.

Figure 4 shows a comparison of our predictions for excitation of the $(5s)^2S_{1/2} \rightarrow (5p)^2P$ transition without resolving the fine-structure of the two final states. The insert depicts the small-angle region, where some differences can actually be noticed. These are due to the slightly different oscillator strengths in the various calculations. Recall that the oscillator strength was used to put the experimental data on an absolute scale. Ultimately, it is hard to judge the various datasets based solely on the angular dependence of the experimental data, whose drop-off with increasing scattering angle appears to be less steep than in most theories. The DBSR models give an oscillator strength of 1.0269 for the unresolved transition, which is very close to the likely most accurate value of 1.0231 [18]. Hence, if a decision had to be made, one might want to give the highest weight to the DBSR predictions. The two distorted-wave models (nonrelativistic DWBA and relativistic RDW) appear to have too large values of the optical oscillator strengths in their structure description, which then leads to a likely overestimate of the DCS in the small-angle region. The DWBA and RDW results also differ significantly from each other as well as the other datasets for the larger angles, with the DWBA being almost flat and the RDW showing a clear minimum in the 140–150° range.

5 Conclusions

We have reported results from a number of theoretical models for electron-impact excitation of the $5\,^2S_{1/2} \rightarrow 5\,^2P_{1/2}$ and $5\,^2S_{1/2} \rightarrow 5\,^2P_{3/2}$ resonance transitions in rubidium by 40 eV incident electrons. The results were compared with each other as well as an, unfortunately, limited set of experimental data in the angular range of 2–10° without resolving the fine-structure of the excited-state manifold. Even though a definite conclusion cannot be drawn at this time, experience suggests that the full-relativistic Dirac B-Spline R-matrix models with 150 and 325 states, respectively, yield the most accurate results and hence should be used in any extensive modelling applications.

Data Availability Statement This manuscript has no associated data or the data will not be deposited. [Authors' comment: Data will be made available on reasonable request.].

References

1. L. Vušković, L. Mapeki, S. Trajmar, J. Phys. B **17**, 2519 (1984)
2. H. Tanaka, M.J. Brunger, L. Campbell, H. Kato, M. Hoshino, A.R.P. Rau, Rev. Mod. Phys. **88**, 025004 (2016)

3. B.P. Marinković, R. Panajotović, D. Šević, R.P. McEachran, G. García, F. Blanco, M.J. Brunger, Phys. Rev. A **99**, 062702 (2019)
4. B. Predojević, D. Šević, B.P. Marinković, R.P. McEachran, F. Blanco, G. García, M.J. Brunger, Phys. Rev. A **101**, 032704 (2020)
5. A.V. Pangatiwar, R. Srivastava, J. Phys. B **21**, 4007 (1988)
6. S. Saxena, R. Srivastava, Eur. Phys. J. D **30**, 23 (2004)
7. V. Zeman, R.P. McEachran, A.D. Stauffer, Eur. Phys. J. D **1**, 117 (1988)
8. B.V. Hall, Y. Shen, A.J. Murray, M.C. Standage, W.R. MacGillivray, I. Bray, J. Phys. B **37**, 1113 (2004)
9. W.E. Guinea, G.F. Hanne, M.R. Went, M.L. Daniell, M.A. Stevenson, K. Bartschat, D. Payne, W.R. MacGillivray, B. Lohmann, J. Phys. B **38**, 3359 (2005)
10. D. Payne, B. Krueger, K. Bartschat, J. Phys. B **38**, 3349 (2005)
11. J.H. Chin, K. Ratnavelu, Y. Zhou, Eur. Phys. J. D **68**, 141 (2014)
12. M.A. Haynes, B. Lohmann, I. Bray, K. Bartschat, Phys. Rev. A **69**, 44704 (2004)
13. W. Goldshlag, R. Su, S. Park, J.G. Eden, J. Phys. B **54**, 165001 (2021)
14. C. Perrella, H.P. Griesser, P.S. Light, R. Kostecki, T.M. Stace, H. Ebendorff-Heidepriem, T.M. Munro, A.G. White, A.N. Luiten, Phys. Rev. Appl. **4**, 014013 (2015)
15. B.P. Marinković, S.D. Tošić, D. Šević, R.P. McEachran, F. Blanco, G. García, M.J. Brunger, Phys. Rev. A **104**, 022808 (2021)
16. R.T. Brinkman, S. Trajmar, J. Phys. E **14**, 245 (1981)
17. N.B. Avdonina, Z. Felfli, A.Z. Msezane, J. Phys. B **30**, 2591 (1997)
18. http://www.udel.edu/atom/
19. http://steck.us/alkalidata
20. A. Dalgarno, W.D. Davison, Mol. Phys. **13**, 479 (1967)
21. O. Zatsarinny, K. Bartschat, Phys. Rev. A **77**, 062701 (2008)
22. A. Borovik, V. Roman, O. Zatsarinny, K. Bartschat, J. Phys. B **46**, 015203 (2012)
23. C. Froese Fischer, O. Zatsarinny, Comput. Phys. Commun. **180**, 879 (2009)
24. O. Zatsarinny, K. Bartschat, N.Y. Babaeva, M.J. Kushner, Plasma Sources Sci. Technol. **23**, 035011 (2014)
25. P.J.O. Teubner, J.L. Riley, M.J. Brunger, S.J. Buckman, J. Phys. B **19**, 3313 (1986)
26. M.J. Brunger, J.L. Riley, R.E. Scholten, P.J.O. Teubner, J. Phys. B **21**, 1639 (1988)
27. K.R. Hamilton, O. Zatsarinny, K. Bartschat, M.S. Rabasović, D. Šević, B.P. Marinković, S. Dujko, J. Atić, D.V. Fursa, I. Bray et al., Phys. Rev. A **102**, 022801 (2020)
28. B.H. Bransden, C.J. Joachain, *Physics of Atoms and Molecules* (Longman Group Ltd., London, New York, 1983)
29. K. Bartschat, N.S. Scott, Comput. Phys. Commun. **30**, 369 (1983)
30. K. Bartschat, Comput. Phys. Commun. **30**, 383 (1983)
31. K. Bartschat, K. Blum, J. Phys. B **15**, 2747 (1982)
32. W. Eitel, J. Kessler, Phys. Rev. Lett. **24**, 1472 (1970)
33. V.I. Kelemen, Tech. Phys. **49**, 661 (2004)
34. A. Sakaamini, J.B. Faure, M.A. Khakoo, O.I. Zatsarinny, K. Bartschat, Atoms **9**, 61 (2021)
35. A. Sakaamini, J.B. Faure, M.A. Khakoo, O. Zatsarinny, K. Bartschat, Phys. Rev. A **104**, 062805 (2021)